Flame Height Effects on Agglomerate Size in Aluminized Solid Propellants

Stefano DOSSI, Filippo MAGGI*, and Luigi T. DE LUCA**
**Politecnico di Milano, Department of Aerospace Science and Technology*
34, Via La Masa, 20156, Milan, Italy

Abstract

Solid rocket motors are one of the most used systems for space propulsion. Along with the numbers of advantages like simplicity, low cost, technological maturity and high thrust, this propulsion system exhibits relatively low gravimetric specific impulse among the thermochemical engine family. When metallized, solid propellants release droplets of molten aluminum (agglomerates) causing a further reduction of performance. This phenomenon depends on several parameters (e.g. burning rate, microstructure, propellant formulation, flame position, local temperatures etc.). This work focalizes the attention on the relation between agglomerate size and flame height. A theoretical investigation has been performed to select five representative formulations. An experimental campaign has been performed to characterize the materials in terms of burning rate, agglomerate size, and density. A simple code based on the GDF theory has been used to compute the flame height of interested formulations. Numerical and experimental data have been finally compared revealing a linear dependence of agglomerate size on the flame height, thus confirming the key role played by the flame in agglomerate growing and formation.

1. Introduction

Metal powders (e.g. Al, Be, Zr, Mg, b, etc.) are of primary importance for solid propulsion, improving the specific impulse of solid rocket motors (SRMs) by increment of not only the combustion temperature, but also the propellant density [1]. In this respect, micrometric aluminum (μAl) is one of the most used ingredients thanks to its intrinsic properties like stability, low cost, low toxicity and easy handling.

From a propulsive point of view, the use of low reactive metal fuels, such as μAl, is responsible for a consistent reduction of the ideal specific impulse, due to the presence of condensed combustion products (CCPs) expanding through the gas-dynamic nozzle. The presence of burning droplets of molten Al (agglomerates), in the solid rocket core flow causes a detriment of the ideal specific impulse ranging from 1% to 3% [2]. In solid rocket motors, this loss represents about the 35% of the total decrement of the ideal specific impulse. Size and mass fraction of CCPs have been found to be relevant parameters for performance detriments due to thermal and velocity lag of condensed particles [2] [3]. The relevance of micrometric aluminum behavior during combustion led to a strong effort of the scientific community in increasing its comprehension, as testified by the number of authors working on this topic.

1.1 Aluminum ignition temperature and burning time

The burning time of aluminum particles having different size was extensively discussed by Beckstead [4]. His work offered an excellent interpretation of ignition data obtained by several authors using different particle size and atmospheres, highlighting the importance of both the parameters. For the investigated range (above 15 μm), the trend of burning time as a function of initial diameter approached the D^2 law, typical for diffusive combustion regime of droplets [5]. Actually, the exponent was found to be slightly lower, due to the growth of the oxide cap on top of the particle. Despite the effect of the specific composition of the ambient gas, the burning time was found to be weakly dependent on pressure and temperature [6].

For micrometric ingredients most of the available works testify that the ignition temperature (T_{ign}) is strongly dependent not only on the granule size, but also on the sample heating rate. T_{ign} is around the melting temperature of alumina (2323 K) for particles larger than 100 μm and between 1300 K and 2300 K for granules of 1 μm - 100 μm [7]. This behavior is related to the strong thermal capacity of micrometric particles. During heating, the Al core

expansion causes the rupture of the external oxide layer exposing the Al to the oxidizing gases. However, the energy obtained by combustion is not sufficient to increase the temperature of the particle leading to a self-sustained reaction. The result is a sort of self-repairing process during which the oxidized spilled aluminum seals the cracks. Dependence of T_{ign} on the heating rate has been also found as testified by Trunov et al. in [8]. A certain influence on the ignition temperature is also associated to the specific particle shape. Strongly irregular particles exhibit a lower T_{ign} with respect to big granules as evidenced in [9].

1.2 Genesis and structure of agglomerates in AP-based solid propellants

Formation and evolution of agglomerates have been widely studied in several countries (from USA to Russia). An excellent survey concerning structure, formation and size of agglomerates has been carried out by Babuk et al. in [10][11] [12][13][14]. Agglomerates were divided into two categories: non spherical particles, composed by aluminum, alumina and other materials like partially pyrolyzed binder and oxidizer, and spherical objects containing only aluminum and alumina. Both the categories were observed experimentally, but the second one was found to be prevalent for a variety of solid propellants and a wide range of burning conditions [11]. The presence of the skeleton layer (SL) was considered the basic condition for the formation of agglomerates [10][13]. This peculiar structure, permeable to gases, generates on the propellant combustion surface and is composed by aluminum, alumina, and partially by carbonaceous elements. The main SL feature is the adherence of the Al granule assuring the existence of the two most important factors for agglomeration: retention and contact between particles [11][14]. Agglomerates are generated on the top surface of the skeleton layer and their properties depend on the features of the emerging primary particles as well as on their evolution (particle coalescence, physicochemical transformation inside the agglomerate, metal combustion, etc.) [12]. The layout of the skeleton layer depends on propellant microstructure, a concept introduced by Price and well explained in [15]. In AP-based propellants, the coarse granules of oxidizer delimit fuel rich regions called pocket. A pocket is mainly composed by Al, binder and, if present, by the fine fraction of the oxidizer. These structures are connected by thin regions called bridges. In AP/HTPB-based propellants, the SL is formed only within pockets evidencing the strong connection between agglomeration and propellant microstructure [13][14]. Babuk underlines the effects of pressure and propellant family not only on the agglomerate structure, but also on their size and quantity [10][11][12][13][14]. An extensive study based on the collection of CCPs by mean of a quenching plate or a liquid quenching pool has been carried out demonstrating the positive effect of increasing pressure in reducing the size of agglomerates [11]. The importance of microstructure and pressure is also demonstrated by the dependence of agglomerate size and quantities on the agglomeration regime (sub-pocket, pocket, inter-pocket) [11][12][14]. The presence of both inter-pocket and pocket regimes is typical of low combustion pressures or, in general, slow-burning propellants. In the former regime, the whole amount of Al contained in the pocket takes part to agglomeration process, while in the latter the agglomerate remains on the propellant burning surface accumulating Al from other pockets and increasing its size. The inter-pocket regime can lead to the formation of “matrix” agglomerates, characterized by a sphere of alumina incorporating aluminum droplets [13][14]. Increasing pressure, the inter-pocket regime tends to disappear and agglomeration occurs only in the pocket and sub-pocket regime. The sub-pocket regime is typical of fast-burning propellants or high combustion pressures. In this case, the agglomerate is composed only by a portion of the aluminum contained into the pocket leading to a reduction of the average agglomerate size.

An extensive description of agglomeration and pre-agglomeration behavior of Al has been carried out also by Price et al. in [15][16][17][18]. These authors recognized the importance of the propellant microstructure underlining that the size of ingredients (oxidizer and Al powder) influences the size of agglomerates. Aluminum and fine oxidizer particles were considered as immersed in a “binder sponge” composed by the coarse AP fraction (AP_c). Coarse oxidizer particles generate fuel rich regions in a material that is already fuel rich. It is clear that this description perfectly fits with the concept of microstructure. During propellant combustion, aluminum was observed to accumulate on the burning surface. In AP-based propellants, a prompt ignition is prevented by the presence of the oxide shell protecting Al particles and by the low local concentration of oxidizing species. Al clusters have been evidenced through visualization and quenching tests testifying the presence of sintering processes caused by the leakage of molten aluminum throughout cracks in the alumina shell. Price et al. related the size of accumulates to the propellant microstructure (pocket size) and to the conditions causing their adherence to the propellant surface. Notice that this condition does not allow the ignition of the accumulate [16]. The ignition process occurs when the accumulate is well exposed to the diffusion flame of the propellant (AP-binder flame) and is described as a progressive auto-accelerated process called inflammation causing the coalescence of the accumulate into a burning sphere of molten aluminum. A detailed sketch of a single agglomerate showing its typical structure was given by Price in [16] and [17]. After the formation, an agglomerate is composed by an aluminum droplet (showing a characteristic spherical shape), an oxide lobe, and other substances coming from the pyrolysis of the binder. The sphere is surrounded by a visible plum following the gaseous flow coming from the propellant. Again the size of

agglomerates was found to be dependent on the propellant microstructure and pressure regime, thus confirming what observed by Babuk in [11][12][13][14].
All the observations concerning genesis and structure of agglomerates have been also confirmed at SPLab by De Luca et al. and Maggi et al. looking the evolution of solid propellant combustion surfaces with a high speed camera [19][20][21][22]. Effects of pressure, microstructure and propellant formulation on the size of agglomerates have been verified as well.

1.3 Heterogeneity model and agglomeration

A first attempt in relating agglomeration and propellant microstructure was carried out by Povinelli in [23]. CCP particle size was associated to the average distance separating oxidizer particles. Some years later, a model based on the pocket concept was presented by Choen in [24]. In the work, the pocket volume was related to the fraction of agglomerated Al. Two years earlier, another agglomeration model based on ingredient packing was presented in Russia by Grigor'ev et al [25]. In 1999, Babuk underlined the role of the coarse oxidizer fraction and the final size of CCP by using a large set of experimental data [11][13]. More recently, Rashkovskii worked on a model relating the average size of agglomerates with the structure and size of Al particle clusters forming during heterogeneous condensed mixture combustion [26]. The model was based on the statistics of simulated propellants allowing a direct comparison between microstructure and agglomeration. Almost in the same period, Jackson worked on three agglomeration models considering different geometrical domains. The propellant heterogeneity was simulated by a random pack of aluminum and AP particles [27]. The use of a pocket model to correlate propellant microstructure and agglomerate size have been carried out by Gallier in [28]. The model estimated agglomerate fraction and diameter by using a second order statistics. A similar approach has been used also by Maggi et al. in [19][20][30]. The first work evidenced the dependence of agglomerate size on propellant microstructure by correlating CCP average diameter with the collection radius obtained by a packing model. In [20], a series of experimental results was compared with agglomerate size obtained through a numerical approach. More details concerning the packing code used in the two works are reported in [29]. In [30], an automated measuring method for agglomerates and a novel agglomeration model were described. In this case, the attempt was to compare experimental and numerical CCP size distributions. Despite a global similarity, the presented model showed the tendency of over-estimating the central part of the actual CCP size distribution. An excellent attempt to relate propellant heterogeneity and flame structure to the size of CCPs was carried out by Srinivas et al. in [31]. The proposed algorithm modeled the propellant structure by random pack of ingredients. Al particles were tracked and their accumulation on burning surface was simulated. The ignition occurred by the effect of leading edge oxidizer-binder diffusion flamelets (LEF). The ignition delay was computed by a heat transfer model and was responsible for the final agglomerate size. Comparison between numerical and experimental data shown the dependence of agglomerate size and LEF by the pressure.

1.4 Target of the work

With some differences, most researchers agree in defining the heterogeneity and the flame structure as the two most important parameters driving the agglomeration phenomenon. The former is responsible for the size of the initial cluster of Al and then, partially, for the diameter of condensed combustion products; the latter drives the ignition of the accumulate influencing the inflammation delay and then the formation and the size of agglomerates. In this respect, we should remember that the propellant microstructure is defined by ingredient size and mixing procedure while the flame structure is strongly affected by the burning pressure. The interdependence of these parameters seems to be ascertained; however it should be confirmed by a definitive relation. The target of this work is to verify the existence of a clear connection between agglomerate size and propellant flame. A series of AP/HTPB-based propellants have been manufactured and burned to obtain the burning rate (r_b) and the average agglomerate size. The propellant flame height has been estimated applying the granular diffusion flame (GDF) model starting from experimental data. The two parameters have been finally compared.

2. Propellant selection

The selection of propellant formulations has been executed by applying both spatial statistics and thermochemistry of the pocket. The former approach allows to define the average pocket size of the propellant, while the latter offers a global overview concerning the local flame temperature of the system. A detailed description of the selection procedure is reported in [32]; here it is presented only a rapid survey.

2.1 Pocket size

The average size of the pocket and its existence limit have been determined by using a packing model. An overall formulation of AP/HTPB/Al 68%/14%/18% has been considered (see Table 1).

Table 1: Model propellant formulations. Fractions are expressed by mass.

ID	AP		Al	Binder
	d = 200 µm	*d < 10µm*	*d = 30 µm*	
AP0	68 %	0 %	18 %	14 %
AP5	63 %	5 %	18 %	14 %
AP10	53 %	10 %	18 %	14 %
AP20	48 %	20 %	18 %	14 %
AP30	38 %	30 %	18 %	14 %
AP40	28 %	40 %	18 %	14 %
AP50	18 %	50 %	18 %	14 %

Since the propellant microstructure is described by the coarse AP fraction (AP_c) , the fine AP fraction (AP_f) has been considered perfectly homogenized into the binder. The change of the pocket size has been obtained by substituting the coarse AP with the fine AP, keeping the same amount of oxidizer. The packing code is based on the Lubachevsky-Stillinger algorithm and assumed spherical objects only. For each analysis, the partial radial distribution function (RDF) was monitored. The RDF is a second order statistical descriptor allowing the computation of pocket size. In this case, the function is specialized on Al particles, following a statistical pocket model developed by Maggi and co-authors [19]. Since a pocket is surrounded by a boundary of AP particle, there is a region in which the number of aluminum granules is low. This condition, defining the pocket border, is identified by the first minimum of the function located below the unity. Figure 1 reports the RDF of the model propellants enlisted in Table 1. The first minimum of the RDF (below the unity) tends to shift towards higher values of the radius when the content of fine AP is increased. Similarly, the minimum can be found for a RDF value as close to one as AP_f increases. For a fine AP content of 50 %, the RDF function does not assume values below one, evidencing the impossibility to define anymore the pocket concept. For this reason, this particular composition has been discarded.

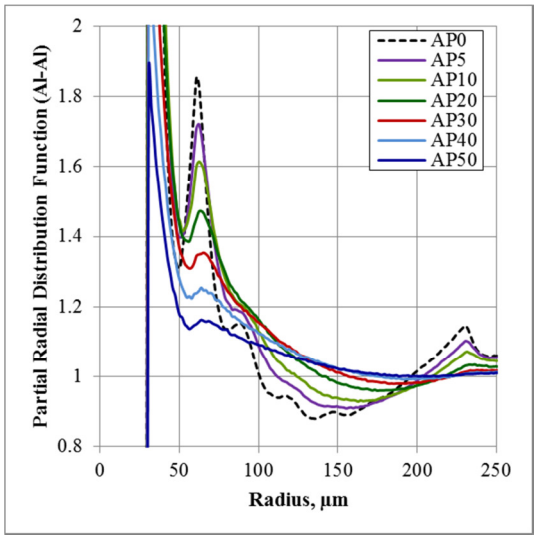

Figure 1: Partial Radial Distribution Function for model propellants of Table 1. The shift of the first minimum value below the unity is observed.

2.2 Pocket adiabatic flame temperature

The structure of a heterogeneous material is strongly influenced by the size of the ingredients. Thermochemistry is not able to distinguish between coarse and fine ingredients; however, effects of heterogeneity can be taken into account looking at the specific formulation of the pocket. The pocket can be studied by thermochemistry if treated as a pseudo-propellant, having a different formulation with respect to the original material. Only the binder, the metal,

and, if present, the fine AP fraction take part to it. Figure 2 reports the pocket adiabatic flame temperature (T_{ad-p}) of a solid propellant (AP/HTPB/Al 68%/14%/18%) containing different mass fractions of fine AP. Results are obtained assuming Al as an inert substance. This hypothesis is confirmed by combustion videos in which, after the formation, no appreciable consumption of agglomerates can be observed. This means that the contribution to combustion given by Al is negligible near the burning surface. The pocket adiabatic flame temperature increases from 700 K to 1300 K relatively slowly to strongly accelerate from 1300 K to 2300 K. The plateau located at low AP_f is caused by the melting of aluminum and represents an interesting region to study.

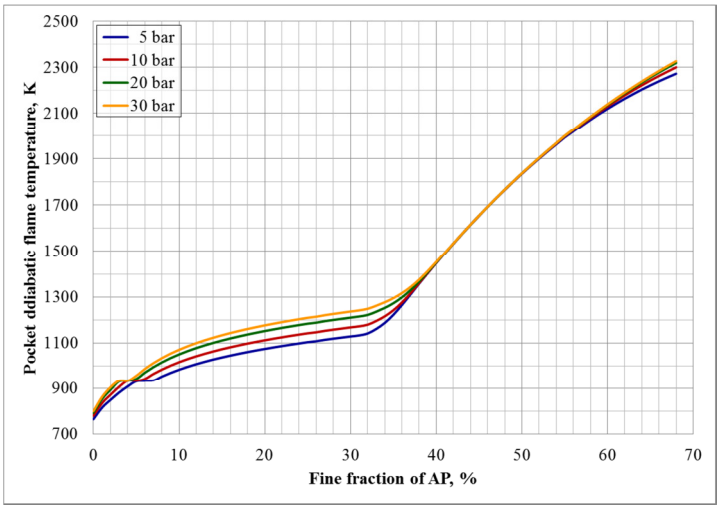

Figure 2. Dependence of the pocket adiabatic flame temperature on the fine AP mass fraction for a composite solid rocket propellant (AP/HTPB/Al 68%/14%/18%) at different pressure regimes. Al is considered inert.

3. Propellant experimental analysis

The most interesting propellant formulations were selected out of Table 1 to guarantee the variation of the microstructure and the most interesting pocket adiabatic flame temperatures. Choices are justified in Table 2.

Table 2: propellant formulations selected for the experimental campaign. Justification of the choices are reported.

ID	AP		Al	Binder	Selection motivation
	d = 200 μm	*d < 10 μm*	*d = 30 μm*		
AP0	68 %	0 %	18 %	14 %	Baseline
AP5	63 %	5 %	18 %	14 %	Plateau of T_{ad-p}
AP10	53 %	10 %	18 %	14 %	Located immediately after the plateau of T_{ad-p}
AP20	48 %	20 %	18 %	14 %	Located in the middle of the slow increasing T_{ad-p} region
AP40	28 %	40 %	18 %	14 %	Maximum allowable AP_f to define the geometry of the pocket

Propellants were produced by a lab-scale technique employing a mechanical mixer. Propulsion-grade Al and AP from an industrial supplier were used. The inert binder, based on HTPB R-45 polymer, was cured by an isocyanate. Propellants were characterized in terms of density, ballistics and CCP size from 5 bar to 30 bar. The experimental set-up for sample combustion was the same used to obtain burning rate and CCP size. It was based on a 2 l combustion chamber equipped with four optical accesses for video recording. The strand burner was pressurized by nitrogen. A set of solenoid valves operated by an analogical regulator was used to keep the pressure constant. Propellant burning rates were measured by analyzing the combustion videos with an internal standardized digital technique. At least three good tests for each desired pressures were executed. Agglomeration videos were recorded with a fast and high-resolution video camera to appreciate all the events occurring on the propellant burning surface. Sample shape was adapted in order to guarantee the best video quality and clearness. Three videos for each pressure were recorded and manually analyzed by ImageJ to obtain the size of at least 200 incipient agglomerates per video (600 diameters for each pressure). The picking procedure was executed by following a consolidated procedure for

recognition and measuring of agglomerates, described in [30].The data set was then elaborated to obtain the mass weighted mean diameter (D_{43}).

3.1 Density and ballistic

As testified by Table 3, the addition of a fine fraction of AP causes an increment of the propellant density probably due to a higher packing efficiency. The theoretical maximum density (TMD) and the density ratio to TMD are also reported.

Table 3: Density of selected solid propellants

Label	Density, ρ, g/cm^3	TMD, g/cm^3	ρ/TMD,%
AP0	1.713	1.761	97.3
AP5	1.718	1.761	97.6
AP10	1.722	1.761	97.8
AP20	1.726	1.761	98.0
AP40	1.728	1.761	98.1

The Vieille's laws ($r_b = a \cdot p^n$) of the tested propellants are sketched in Figure 3. As expected by literature [33], the pressure exponent increases raising the fraction of fine AP (that is diminishing the average size of the oxidizer). The baseline, loaded with coarse AP only, is the slowest propellant, while the material containing the highest amount of fine oxidizer (AP40) features the highest burning rate, especially at high pressure. Surprisingly, sensible changes of the regression rate have not been observed across the entire pressure range using a fraction of fine AP between 5% and 20%.

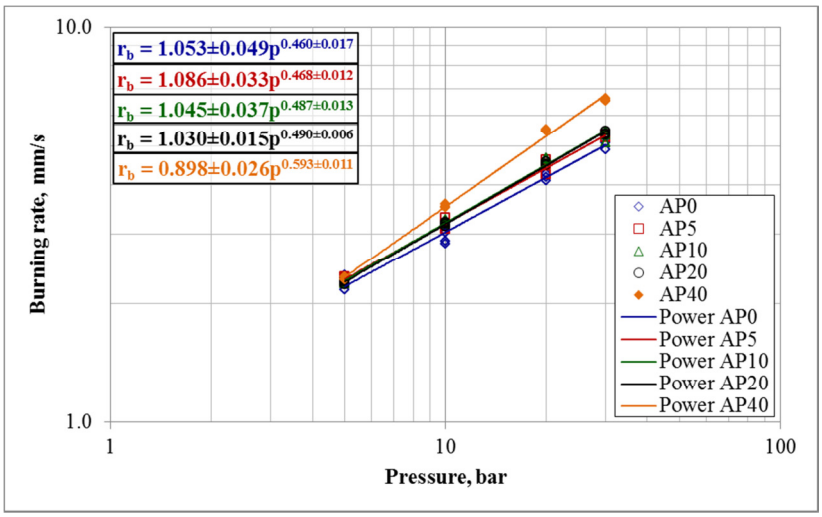

Figure 3: Effects of fine AP mass fraction on propellant ballistic

3.2 Agglomerate size

Agglomeration data for the five tested propellants are shown in Figure 4. A strong reduction of the mass weighted mean diameter is featured increasing the burning pressure independently on the specific material. It is interesting to notice that the addition of fine oxidizer does not cause an immediate reduction of agglomerate size. Conversely, it produces an initial size increment followed by a progressive abatement of the average diameter [32]. The diminishing trend can be successfully approximated by a power law as evident from Figure 4. The smallest agglomerates are found for the propellant AP40 while samples AP10 and AP5, practically exhibiting the same D_{43}, shows the largest CCP size. A midway behavior can be observed for the baseline propellant (AP0).

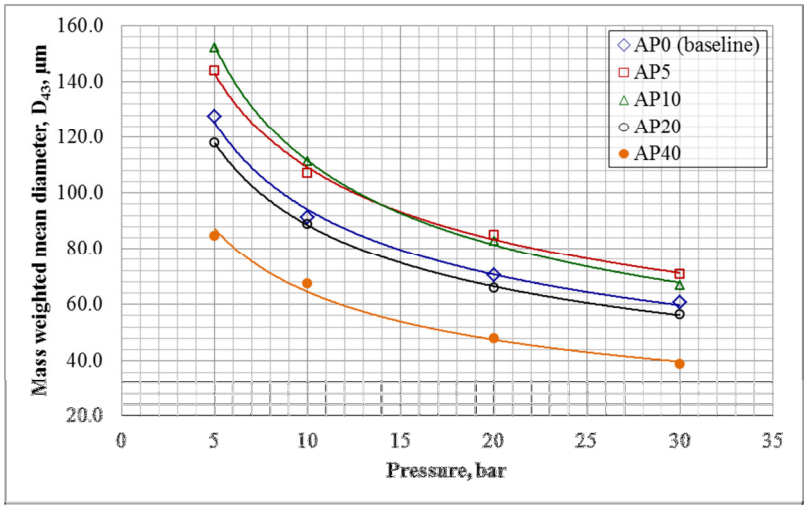

Figure 4: Agglomerate mass weighted mean diameter for tested propellants

4. Propellant flame height

The flame height of composite solid propellants has been computed by the granular diffusion flame (GDF) model, using experimental values of propellant surface temperature and burning rate. The original model, described in [34] and [35], was capable of determining a series of parameters (e.g. the burning rate and the flame height) through an iterative process. The reader should note that the GDF model does not fully describe the flame structure, being mono-dimensional, but exploits average propellant features, such as the D_{43} of the oxidizer.

4.1 Model description

The granular diffusion flame model considers three different regions as shown in Figure 5. The first zone (thin for pressure between 1 atm and 100 atm) is defined by the exothermic reaction of ammonia and perchloric acid coming from the sublimation-dissociation of AP. The second zone is characterized by the reaction of fuel and oxidative products coming from the first reaction zone. The last zone is described by the presence of the exhaust gases and is of less importance for the model.

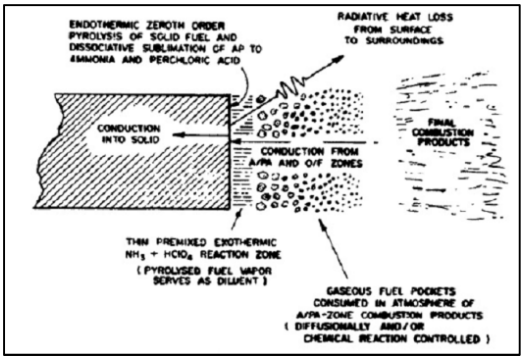

Figure 5: Scheme of the GDF structure [35]

The GDF is based on an energetic approach considering the conduction through the solid propellant, the convection from the two flame zones to the combustion surface and the radiative loss. The entire model is 1D and realized assuming a propellant containing AP as oxidizer and two stationary planar flames parallel with respect to burning surface. The model has two different versions depending on the definition of the first flame zone. If this region is neglected, the model is defined “collapsed”, otherwise it is called “extended”. For the present work, the extended GDF theory was considered. Both the interpretations derive from the same concept.

A rapid explanation of the theory discussed in [35] is reported hereafter. More details can be found in [35] and [36]. The thermal balance on the burning surface lead to the simple equation (1).

$$\rho_c r\left[C_g(T_2 - T_0) + \Delta h_{tr} + \Delta h_s + \Delta h_I + \Delta h_{II}\right] + \epsilon\sigma T_s^4 - \lambda_g \frac{dT}{dx}\Big|_{2,g} = 0, \quad (1)$$

where:

- ρ_c is propellant density,
- r is the propellant burning rate,
- $C_g$is the specific heat of the gas,
- T_0 and T_2 are the temperature of the propellant and at the end of the zone II respectively,
- T_s is the burning surface temperature,
- Δh_{tr} is the transition enthalpy of AP from orthorhombic to cubic structure,
- Δh_s is the dissociation enthalpy of AP,
- Δh_I and Δh_{II} are the enthalpy variation at the end of the zone I and II respectively
- λ_g is the thermal conductivity of the gas phase,
- ϵ is the burning surface emissivity,
- σ is the Stefan-Boltzman constant.

Assuming that all the temperature gradients are linear and equal to zero when the temperature reaches the value T_2, the equation (1) can be simplified in:

$$\rho_c r\left[C_g(T_2 - T_0) + \Delta h_{tr} + \Delta h_s + \Delta h_I + \Delta h_{II}\right] + \epsilon\sigma T_s^4 - \lambda_g \left(\frac{T_2 - T_1}{L_{II}}\right) = 0, \quad (2)$$

where:

- T_1 is the temperature at the end of the zone I,
- L_{II} is the flame height of the zone II.

The parameter r in equations (1) and (2) satisfies the Arrhenius law for the pyrolysis reactions:

$$r = Ae^{\left(-\frac{E_S}{RT_S}\right)} \quad (3)$$

The flame height of the first reaction zone can be computed through the equation (2)

$$L_I = \left(\frac{\rho_c R}{M_1}\right)\frac{rT_1}{P}\tau_I \quad (4)$$

where:

- P is the pressure,
- R is the universal gas constant,
- M_1 is the gas molar mass of the zone I,
- τ_I is the reaction time of the zone I.

The expression for τ_I is obtained considering the reaction $NH_3/HClO_4$ bimolecular of the second order. In this way the reaction time depends only on the pressure (see eq. (5)).

$$\tau_I = 6.5 \cdot 10^{-6} P^{-1} \quad (5)$$

The flame height of the second reaction zone can be expressed similarly to L_I

$$L_{II} = \left(\frac{\rho_c R}{M_2}\right)\frac{rT_2}{P}\tau_{II}. \quad (6)$$

where:

- M_2 is the gas molar mass of the zone II,
- τ_{II} is the reaction time of the zone II.

In this last case, the expression of τ_{II} is more complex:

$$\tau_{II} = \frac{PM_2}{RT_2}\left(\frac{\alpha T_2}{P}e^{\frac{E_2}{2RT_2}} + \frac{\beta(d)T_2^{5/6}}{P^{1/3}\,T_s^{7/8}}\right)^2 \tag{7}$$

where:

- E_2 is the activation energy for the zone 2,
- α and $\beta(d)$ are two constant..

Starting from (2), (6) and (7) , the burning rate can be expressed as:

$$\frac{1}{r} = \rho_c \sqrt{\frac{\left[C_g(T_s - T_0) + \Delta h_{tr} + \Delta h_s + \Delta h_I + \Delta h_{II} + \frac{\epsilon\sigma T_s^4}{\rho_c r}\right]}{\lambda_g(T_2 - T_s)}}\left\{\frac{\alpha T_2}{P}e^{\frac{E_2}{2RT_2}} + \frac{\beta(d)T_2^{5/6}}{P^{1/3}\,T_s^{7/8}}\right\} \tag{8}$$

If we consider the surface temperature of the propellant constant and neglecting the radiative heat losses, equation (8) can be rewritten as:

$$\frac{1}{r} = \frac{a}{P} + \frac{b(d)}{P^{1/3}} \tag{9}$$

where:

- a is the chemical reaction time parameter,
- $b(d)$ is the diffusion time parameter.

From eq. (3), (8) and (9) and noticing that a and $b(d)$ can be obtained from experimental regression rates, it is possible to obtain α and $\beta(d)$. The exact value of T_2 can be determined starting from the adiabatic flame temperature $T_{2(ad)}$ by the following expression:

$$T_2 = T_{2(ad)} - [\epsilon\sigma T_s^4 e^{\left(\frac{E_s}{RT_s}\right)}]/(\rho_c C_g A) \tag{10}$$

In this work, both the burning rate and the surface temperature are input parameters known from experiments. Under this assumption, the model can be rewritten in a reduced form. Eq. (7) becomes

$$\tau_{II} = \frac{PM_2}{RT_2\rho_c^2}\left[\frac{\lambda_g(T_2 - T_s)}{C_g(T_s - T_0) + \Delta h_{tr} + \Delta h_s + \Delta h_I + \Delta h_{II} + \frac{\epsilon\sigma T_s^4}{\rho_c r}}\right]\frac{1}{r^2} = \frac{PM_2}{RT_2\rho_c^2}D\frac{1}{r^2} \tag{11}$$

where

$$D = \frac{\lambda_g(T_2 - T_s)}{C_g(T_s - T_0) + \Delta h_{tr} + \Delta h_s + \Delta h_I + \Delta h_{II} + \frac{\epsilon\sigma T_s^4}{\rho_c r}} \tag{12}$$

The final relation to compute the flame height of the second reaction zone can be easily obtained by combining eq. (6) and (11)

$$L_{II} = \frac{1}{\rho_c}D\frac{1}{r} = \frac{1}{\rho_c}\left[\frac{\lambda_g(T_2 - T_s)}{C_g(T_s - T_0) + \Delta h_{tr} + \Delta h_s + \Delta h_I + \Delta h_{II} + \frac{\epsilon\sigma T_s^4}{\rho_c r}}\right]\frac{1}{r} \tag{13}$$

Obviously, the final flame height is computed as:

$$L = L_I + L_{II} \tag{14}$$

This reduced version of the GDF is valid only if the burning rate and the surface temperature of the interested propellant are known.

4.2 Application limits

The application limits for the GDF theory were clarified in [35] by the authors. The strongest concern was related to the loss of the hypothesis of mono-dimensionality. This circumstance can be reached when the flame height becomes comparable to the combustion surface roughness so that the flame can no more be considered planar. Both the increment of pressure and oxidizer diameter can lead to the presented situation. According to Summerfield and colleagues, the model is applicable for AP-based solid propellants loaded with non-readily melting binders. The theory is valid in the range of 1-100 atm and for an average oxidizer particle size below 250 μm. Moreover, the following relation has to be verified:

$$\psi_0 \geq 0.58 - 0.10 \log_{10}(d_{AP}) = \psi_p \tag{15}$$

where:

- ψ_0 (= 0.538 for the considered formulation) is defined as the ratio between the oxidizer to fuel mass ratio and the oxidizer to fuel mass ratio in stoichiometric conditions,
- d_{AP} is the oxidizer average diameter.

Table 4: Check for the GDF applicability with the tested propellants

Propellant label	d_{AP}, μm	P, bar	ψ_0	ψ_p
AP0	200.0	5-30	0.583	0.350
AP5	186.0	5-30	0.583	0.353
AP10	172.1	5-30	0.583	0.356
AP20	144.1	5-30	0.583	0.364
Ap40	88.2	5-30	0.583	0.385

As evidenced by Table 4, the bonds have been respected and the model is applicable with all the five considered propellants.

With respect to the original model, the propellants considered for this work contains a consistent fraction of micrometric aluminum. Addition of Al was already extensively debated in [35] recognizing some possible effects on propellant combustion. The presence of this metal promotes some contrasting effects. Al, for example, acts as a heat sink, removing energy from the combustion surface. This behavior is emphasized by the melting of Al occurring at 933 K. On the other hand, agglomerates return energy to the solid propellant, burning partially in the flame region and partially in the post-flame zone. From combustion videos recorded at SPLab, it appears that the consumption of the agglomerate trough the flame zone is negligible. If we limit the attention on the region immediately near the propellant, we can then assume that agglomerates pass through the flame zone without reacting and behaving like an inert material. For these reasons, the presence of Al does not represent a problem. The melting enthalpy of the material is obviously considered and inserted into the equations.

4.3 Results

To obtain the solution using the reduced form of the GDF, it is necessary to know the surface temperature of the propellant. T_s values are taken considering the Arrhenius's law proposed in [37] by Zanotti et al. starting from experimental tests:

$$r_b = A_p e^{\left(-\frac{E_p}{RT_s}\right)} \tag{16}$$

where:

- A_p is the pre-exponential factor equal to 127772 cm/s ,
- E_p is the activation energy for a AP/HTPB/Al 68%/14%/18% propellant (22187 cal/mol).

Both the two values were obtained by digitalization of the r_b-to-$(1/T_s)$ graph for the interested propellant (see [37]). Other values used in the model for the computation of the flame height are reported in Table 5 and were derived from [35] or obtained by CEA.

Table 5: Values used for the determination of the flame height

Symbol	Description	Value	Pressure, bar
Δh_{tr}	AP transition enthalpy, cal/g	20.0	-
Δh_s	AP dissociation enthalpy, cal/g	520.0	-
Δh_b	Binder decomposition enthalpy, cal/g	66.1	-
Δh_{Al}	Al melting enthalpy, cal/g	94.4	-
Δh_I	Enthalpy at the end of the zone I	-800.0	-
ϵ	Propellant emissivity	0.75	-
T_0	Reference temperature, K	300.0	-
T_{2ad}	Adiabatic flame temperature at the end of the zone II, K	2272.3	5
		2300.6	10
		2319.2	20
		2327.0	30
C_g	Burned gas specific heat, cal/g/K	0.4543	5
		0.4550	10
		0.4558	20
		0.4561	30
λ_g	Gas thermal conductivity, cal/cm/s/K	$6.03 \cdot 10^{-4}$	5
		$5.99 \cdot 10^{-4}$	10
		$5.93 \cdot 10^{-4}$	20
		$5.90 \cdot 10^{-4}$	30
ρ_c	Propellant density	See Table 3	-
$M_2 = M_1$	Burned gas molar mass, g/mol	28.44	5
		28.57	10
		28.65	20
		28.69	30

Flame height for the tested propellants from 5 bar to 30 bar are sketched in Figure 6. As expected, the propellant loaded with coarse AP exhibits the largest values of the flame height, while the shortest flame is shown by the propellant loaded with 40% of fine AP.

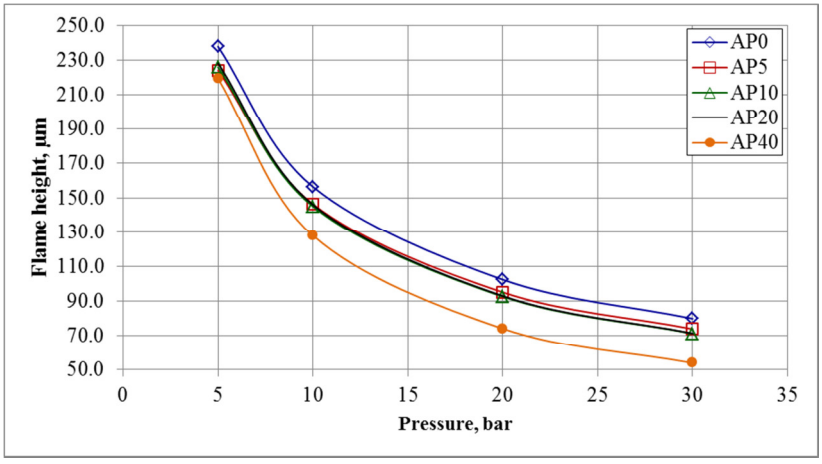

Figure 6: Dependence of the flame height on the pressure, for the tested propellants

4. Discussion

The combined interpretation of experimental data can bring to interesting results. All the propellants exhibits a reduction of the agglomerate mass weighted mean diameter increasing the pressure. This is not a new result and it

was already discussed in other works. Specifically, it was related to an increment of the burning rate combined with a reduced residence time on the propellant combustion surface. However, the increment of the burning rate cannot be considered the sole parameter driving the agglomerate size. From Figure 3 and Figure 4, the absence of a direct connection between the two parameters is evidenced by the fact that fast propellants (AP5 and AP10) exhibit a larger D_{43} for CCP with respect to the slowest propellant AP0. This result is not new too, and was already discussed in [32] and [36]. In [32], this peculiar effect was imputed to the existence of a specific local flame temperature of the pocket (around 900-1000 K) evidencing the important role played by local conditions.

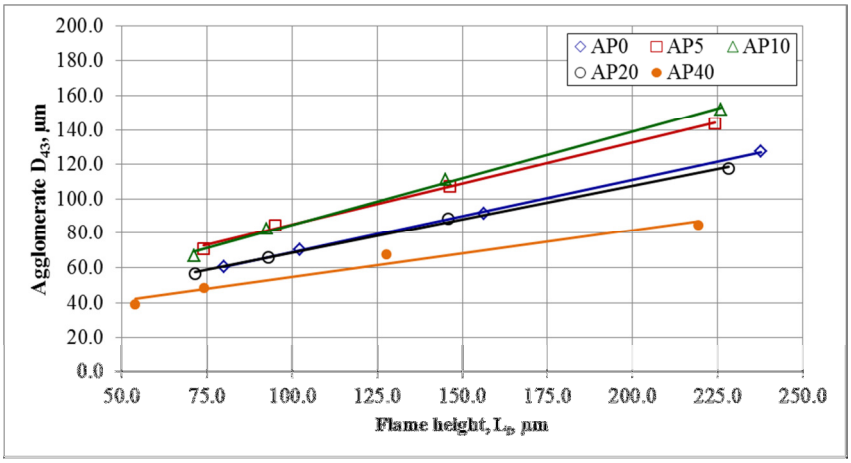

Figure 7: Agglomerate mass weighted mean diameter vs flame height for the tested propellant

Table 6: Fitting line equations and R^2 for propellants of Figure 7

Propellant Label	Fitting line	R^2
AP0	$D_{43} = 0.42 \cdot L_f + 26.62$	0.999
AP5	$D_{43} = 0.48 \cdot L_f + 37.38$	0.997
AP10	$D_{43} = 0.54 \cdot L_f + 30.73$	0.996
AP20	$D_{43} = 0.39 \cdot L_f + 29.56$	0.997
AP40	$D_{43} = 0.27 \cdot L_f + 27.43$	0.965

Particularly interesting is the correlation of the measured incipient agglomerate D_{43} with the flame height. From Figure 7 and Table 6, it is evident that the average size of agglomerates depends linearly on the propellant flame height. This is true for all the tested formulations, thus confirming the existence of a strong correlation between the two parameters.

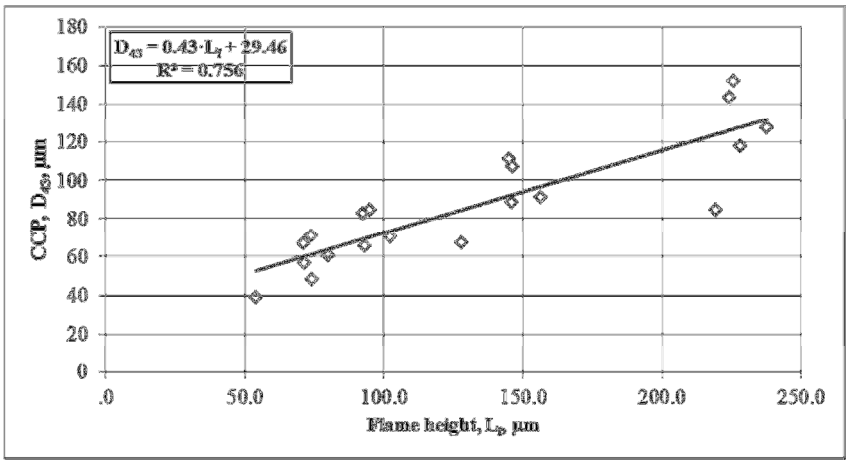

Figure 8: Overall L_f to CCP D_{43} trend

Also the overall comparison reported in Figure 8 suggests a general linear trend. However, the coefficient of determination is relatively low (0.753). In this case, it is necessary to remember that the computation of the flame height has been executed considering a general surface temperature. The flame heights cannot be directly compared since a correction is requested on the basis of the actual surface temperature of each propellant. This parameter could change due to a strong variation of the fine fraction of AP promptly reacting on the burning surface.

5. Conclusions

This work has studied the relation between average agglomerate size and flame height of solid rocket propellants. Investigations have been executed on the same nominal propellant composition (AP//HTPB/Al 68%/14%/18%). Five formulations have been selected based on spatial statistics and thermochemical calculations varying the fraction of fine AP. During preliminary analyses, Al has been considered an inert material capable only to melt and to absorb heat.

A simple code based on the granular diffusion flame model by M. Summerfield has been used to determine the flame height of the interested formulations. The original concept was partially adapted to use experimental data as input parameters and to include the presence of Aluminum. Applicability bounds were described and checked for all the propellants.

The experimental activity was conducted on a series of lab-scale samples to determine density, burning rate and agglomerate average size. The analysis of results brings to the conclusion that agglomeration and flame height are effectively connected. A linear relation between the two parameters has been found for all the tested formulations. In addition, the analysis of the whole result data set featured a linear D_{43}-to-L_f trend. The low value of the correlation coefficient is imputed to the specific propellant surface temperature used for flame height computation. Values were taken considering a general AP/HTPB/Al 68%/14%/18% propellant completely neglecting both microstructure and changes related to the specific formulations.

From experimental result it can be stated that a reduction of the flame height is responsible for the anticipation of the accumulate inflammation accelerating its ignition, thus reducing the final size of the agglomerate. The reduction of the flame height is generally associated to fast propellants. The presence of fast gases released by the sample further help to reduce the residence time of the agglomerate, decreasing its final diameter.

A first extension of the work consists in introducing a direct measurement of propellant surface temperature to compute more precisely the flame height. Effect of the local flame temperature on agglomerate size has been introduced in [32] and [36]; other studies on this topic are strongly desirable in order to introduce a possible combination between local and global flame effects on agglomerate size. The application of this method to formulations loaded with other binders having different pyrolysis surface temperatures is interesting to confirm what observed during this work. Finally, it is clear that only an “averaged approach” has been proposed in this work. Better results could be obtained working with local flame heights and CCP particle size distributions.

References

[1] Sutton, G.P., and O Biblarz. 2010. Rocket Propulsion Elements. John Wiley & Sons. Hoboken, New Jersey, USA.
[2] AGARD. 1986. Performance of Rocket Motors with Metallized Propellants. Agard Advisory Report 230. North Atlantic Treaty Organization.
[3] Hermsen, R. W. 1981. Aluminum Oxide Particle Size for Solid Rocket Motor Performance Prediction. *J. Spacecraft.* 18(6):183-490.
[4] RTO. 2004. A Summary of Aluminum Combustion. Published in: RTO-EN-023. North Atlantic Treaty Organization.
[5] Glassman, I., and R. Yetter. 2008. Combustion. Academic Press. San Diego, California, USA.
[6] Sundaram, D. S., V. Yang, and V. E. Zarko. 2015. Combustion of Nano Aluminum Particles (Review). *Combust., Explos. Shock Waves.* 51(2):37-64.
[7] Yetter, R. A., G. A. Risha, and S. F. Son. 2009. Metal Particle Combustion and Nanotechnology. *Proc. Comb. Inst.* 32(2)-1819-1838.
[8] Trunov, M. A. M. Schoenitz, and E. L. Dreizin. 2005. Ignition of Aluminum Powders on Different Experimental Conditions. *Propell. Explos. Pyrot.*, 1:36-43.

[9] Dossi, S. 2014. Mechanically Activated Al Fuels for High Performance Solid Rocket Propellants. PhD Thesis. Politecnico di Milano, Department of Aerospace Science and Technology.
[10] Babuk, V. A., V. P. Belov, V. V. Khodosov, and G. G. Shelukhin. 1985. Investigation of the Agglomeration of Aluminum Particles During the Combustion of Metallized Composite Condensed Systems. *Combust., Explos. Shock Waves.* 21(3):287-292.
[11] Babuk, V. A., V. A. Vasilyev, and M. S. Malakhov. 1999. Condensed Combustion Products at the Burning Surface of Aluminized Solid Propellant. *J. Propul. Power.* 15(6):783-793.
[12] Babuk, V. A. 2009. Properties of The Surface Layer and Combustion Behavior of Metallized Solid Propellants. *Combust., Explos. Shock Waves.* 45(4):486-494.
[13] Babuk, V. A., V. A. Vassiliev, and V. V. Sviridov. 2000. Formation of Condensed Combustion Products at The Burning Surface of Solid Rocket Propellants. In: *Solid Propellant Chemistry, Combustion, and Motor Interior Ballistics.*749-762.
[14] Babuk, V. A., I. N. Dolotkazin, and A. A. Nizyaev. 2013. Analysis and Synthesis of Solutions for the Agglomeration Process Modeling. In: *Progress in Propulsion Physics 4*. 33-58.
[15] Price, E. W., R. K. Sigman, J. K. Sambamurthi, and C. J. Park. 1982. Behavior of Aluminum in Solid Propellant Combustion. Scientific Report No. ADA118128. Georgia Institute of Technology, School of Aerospace Engineering.
[16] Price, E. W. 1984. Combustion of Metallized propellants. In: *Progress in Aeronautics and Aeronautics.* 479-513.
[17] Price, E. W., W. L. Mayer, W. C. Strahle, S. S. Samant, and E. A. Powell. 1979. The Fire Environment of a Solid Rocket Propellant Burning in Air. Scientific Report No. ADA076941. Georgia Institute of Technology, School of Aerospace Engineering.
[18] Price E. W. and R. K. Sigman. 2000. Combustion of Aluminized Solid Propellants. In: *Solid Propellant Chemistry, Combustion, and Motor Interior Ballistics.*663-687.
[19] Maggi, F., L.T. De Luca, and A. Bandera. 2015. Pocket Model for Aluminum Agglomeration Based on Propellant Microstructure. AIAA J. (in press), DOI: 10.2514/1.J053992.
[20] Maggi, F., A Bandera, L. Galfetti, L. T. de Luca, and T. L. Jackson. 2010. Efficient Solid Rocket Propulsion for Access to Space. *Acta Astronaut.* 66(11-12):1563-1573.
[21] De Luca, L. T., L. Galfetti, G. Colombo, F. Maggi, and A. Bandera. 2010. Microstructure Effects in Aluminized Solid Rocket Propellants. *J. Propul. Power.* 26(4):724-733.
[22] De Luca, L. T., L. Galfetti, F. Severini, L. Meda, G. Marra, A. B. Vorozhtsov, V. S. Sedoi, and V. A. Babuk. 2005. Burning of Nano-Aluminized Composite Rocket Propellants. *Combust., Explos. Shock Waves.* 41(6):680-692.
[23] NASA. 1962. Effect of Oxidizer Particle Size on Additive Agglomeration. NASA Technical Note D-1438. National Aeronautics and Space Administration.
[24] Choen, N. S. 1983. A Pocket Model for Aluminum Agglomeration in Composite Propellants. *AIAA Journal*. 21(5):720-725.
[25] Grigor'ev, V. G., K. P. Kutsenogii, and V. E. Zarko. 1981. Model of Aluminum Agglomeration During the Combustion of a Composite Propellant. *Combust., Explos. Shock Waves.* 17(4):356-363.
[26] Rashkovskii, S.A. 2002. Role of the Structure of Heterogeneous Condensed Mixtures in the Formation of Agglomerates. *Combust., Explos. Shock Waves.* 38(4):435-445.
[27] Jackson, T. L., F. Najjar, and J. Buckmaster. 2005. New Aluminum Agglomeration Models and Their Use in Solid-Propellant-Rocket Simulations. *J. Propul. Power.* 21(5):925-936.
[28] Gallier, S. 2009. A Stochastic Pocket Model for Aluminum Agglomeration in Solid Propellants. *Propellants Explos. Pyrotech.* 34(2):97-105.
[29] Maggi, F., S. Stafford, and T. L. Jackson. 2008. Nature of Packs Used in Propellant Modeling. *Phys. Rev. E: Stat., Nonlinear, Soft Matter Phys.* 77(4).
[30] Maggi, F., A. Bandera, L. T. De Luca, V. Thoorens, J. F. Trubert, and T. L. Jackson. 2011. Agglomeration in Solid Rocket Propellants: novel Experimental and Modeling Methods. In: *Progress in Propulsion Physics 2*. 81-98.
[31] Srinivas, V. and S. R. Chakravarthy. 2007. Computer of Aluminum Agglomeration on Burning Surface of Composite Solid Propellant. *J. Propul. Power.* 23(4):728-736.
[32] Maggi, F., S. Dossi, and L. T. De Luca. 2011. Agglomeration and Pocket Structures in Composites Solid Rocket Propellants. In: *4TH European Conference for Aeronautics and Space Sciences.*
[33] Kubota, N. 2015. Propellants and Explosives: Thermochemical Aspects of Combustion. Wiley-VCH. Weinheim, Germany.
[34] Steinz, J. A., P. L. Stang, and M. Summerfield. 1967. Effects of Oxidizer Particle Size on Composite Solid Propellant Burning: Normal Burning, Plateau Burning, and Intermediate Pressure Extinction. Scientific Report No. ADA952028. Princeton University, Department of Aerospace and Mechanical Science.

[35] Steinz, J. A., P. L. Stang, and M. Summerfield. 1969. The Burning Mechanism of Ammonium Perchlorate-Based Composite Solid Propellants. Scientific Report No. AD688944. Princeton University, Department of Aerospace and Mechanical Science.

[36] Dossi, S. 2011. Effects of the Flame Structure on Agglomeration in Aluminized Heterogeneous Solid Propellants (in Italian). MSc Thesis. Politecnico di Milano, Department of Aerospace Science and Technology.

[37] Zanotti, C., A Volpi, M. Bianchessi, and L. T. De Luca. 1990. Measuring Thermodynamic Properties of Burning Propellants. In: *Progress in Astronautics and Aeronautics 143*, *Nonsteady Burning and Combustion Stability of Solid Propellants*. 145-196.